2012 SCEC Progress Report

Project 12140

Surface Slip during Large Owens Valley Earthquakes: Compilation and Characterization of Geomorphic Offsets using GeoEarthscope Lidar Data

E.K. Haddon[1,*], C.B. Amos[1], and R. Bürgmann[2]

[1]Geology Department
Western Washington University
516 High Street
Bellingham, WA 98225
Phone: (360) 650-3581
Fax: (360) 650-7302
*haddone@students.wwu.edu

[2]Department of Earth and Planetary Science, and
Berkeley Seismological Laboratory
University of California
389 McCone Hall
Berkeley, CA 94720
Phone: (510) 643-9545
Fax: (510) 643-9980

Summary

Advances in our ability to image and analyze active faults using high-resolution lidar provide a unique opportunity to characterize the spatial distribution of slip during large earthquake surface ruptures. For strike-slip faults, along-strike compilation of laterally displaced geomorphic features measured using lidar enables the assessment of surface slip during historical and paleoearthquakes. Here, we test whether surface slip during the 1872 *M*w 7.4 – 7.9 Owens Valley earthquake, one of California's three largest historic ruptures, mimics the displacement during earlier events. We utilize recently developed analysis and processing tools to investigate EarthScope lidar data spanning the ~113-km-long Owens Valley surface rupture. We present 68 new measurements of laterally displaced channels, terrace risers, meander scars, lake shorelines, and fan edges, with offsets up to ~85 m. These data are available for download as a Google Earth .kmz and an ArcGIS shapefile. Where possible, we test the precision of lidar-based measurements by comparing our results to published field estimates of surface slip during this event. Displacements attributed to the most recent event (MRE) range between ~2 and ~8 m, with an average horizontal offset of 5.3 ± 2.0 m, similar to previous field-based estimates. Our along-strike compilation suggests that displacement gradients for the MRE are smooth at the >10 km length scale, in contrast with the distinctly peaked distribution estimated from previous field studies. Progressively larger offsets are attributed to earlier surface ruptures and may imply a similar amount of surface slip to the MRE (~5-6 m). Lateral slip during these events contributes to preliminary peaks in the cumulative offset frequency density at ~12 and ~17 m. The precision of these peaks likely reflects some bias toward well-preserved offsets, since the majority of offset features reflect displacement during the most recent event. As we expand our database of offset measurements and further develop a long-term paleoseismic history, we will test whether or not similar patterns of surface slip are repeated as characteristic earthquakes during surface ruptures on the Owens Valley fault.

Introduction

Quantifying the seismic hazard imposed by an individual fault requires accurate knowledge of the spatial distribution of slip and the timing of past, surface-rupturing earthquakes (WGCEP, 2008). Several recent studies demonstrate the utility of high-spatial resolution lidar topography (Zielke et al., 2010) and satellite imagery (Klinger et al., 2011) for characterizing the slip-per-event during large paleoearthquakes along major, strike-slip faults. Each of these studies relies on careful measurement and reconstruction of laterally offset geomorphic features (e.g., stream channels) displaced during one or more earthquake surface ruptures. By compiling large numbers of these measurements along strike, these authors reveal that the total offsets for landforms of various ages cluster at distinct values, reflecting the cumulative slip and the slip-per-event during past earthquakes. Such constraints on the surface distribution of slip then provide key data for testing whether or not similar patterns of surface slip are repeated as characteristic earthquakes during prior surface ruptures (Sieh, 1996) and guide future paleoseismic and field-based slip-rate studies.

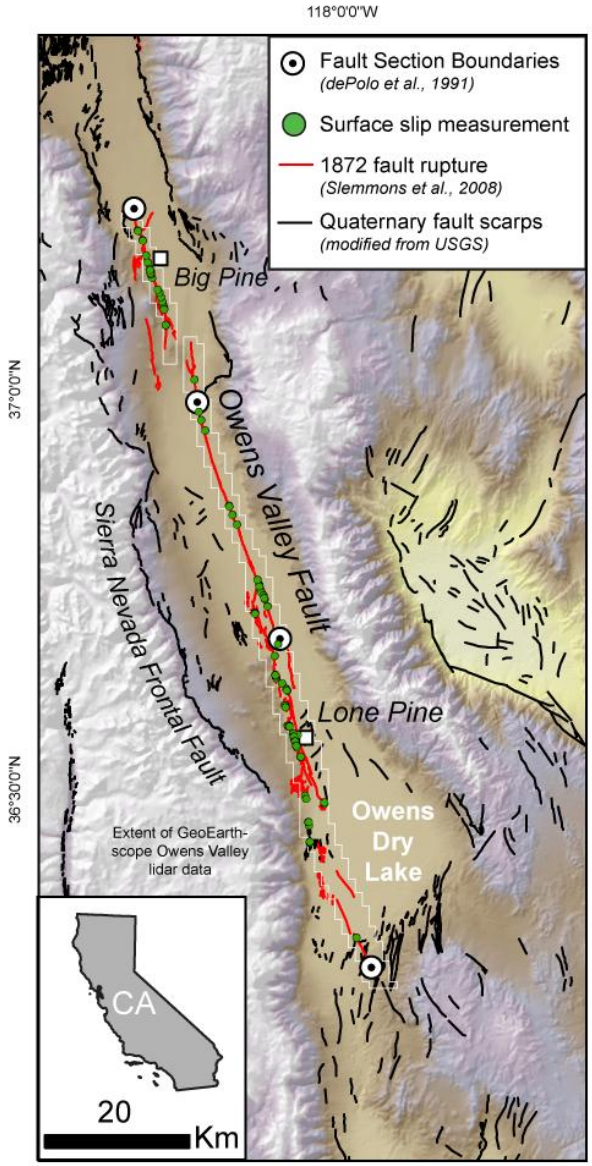

The 1872 M_w 7.4 – 7.9 Owens Valley earthquake ranks among the largest historical earthquake ruptures in California and produced comparable displacement and shaking intensities to the 1906 and 1857 San Andreas earthquakes (Hough and Hutton, 2008). Although field studies document the average amount of surface slip (~6 ± 2 m, Beanland and Clark, 1994), we lacked a comprehensive understanding of how slip during the 1872 earthquake was spatially distributed and have known comparatively little about the cumulative slip caused by earlier events.

Recent availability of high-resolution lidar topography spanning the 1872 Owens Valley surface rupture in southeastern California (Figure 1) enables reevaluation of the amount and extent of surface slip during the 1872 and earlier events. By compiling and cataloging surface slip measurements based on patterns of displaced Quaternary landforms, we produce a new

Figure 1. Regional overview of the ~140 km 1872 Owens Valley earthquake surface rupture including ~100 locations where offset geomorphic features were measured. The white boxes show the areal extent of GeoEarthscope lidar spanning the 1872 surface rupture. Also shown are fault section boundaries inferred by dePolo et al. (1991) based on changes in fault strike and geometric complexity.

database of fault offsets designed to improve our understanding of slip-per-event during Owens Valley earthquakes. This study sheds light on whether previous ruptures produced similar displacements to the 1872 earthquake and allow better characterization of the estimated moment release associated with Owens Valley surface ruptures.

Methods

In order to provide a comprehensive view of surface displacement along strike, we analyzed the entirety of the GeoEarthscope lidar dataset spanning the Owens Valley fault (Figure 1). The remarkably well-preserved and sparsely vegetated geomorphic surface of the arid Owens Valley provides an abundance and diversity of fluvial, lacustrine, and alluvial landforms well suited for lidar analysis. In many locations, several generations of landforms (e.g., debris-flow fans) are cut by the fault and provide measurements of earthquake slip during the 1872 rupture and cumulative slip from earlier events (Figure 2) (Beanland and Clark, 1994; Lee et al., 2001). Given the relatively long recurrence interval (~10 k.y.) estimated for the last 2 – 3 events on the Owens Valley fault (Bacon and Pezzopane, 2007; Bierman et al., 1995; Lubetkin and Clark, 1988), geomorphic surfaces spanning the last ~100 ka (Zehfuss et al., 2001) enable us to extend this paleoseismic record back through the Late Pleistocene.

Our analysis of the Owens Valley lidar data utilizes online tools recently developed and described in Zielke et al. (2010) together with GeoEarthscope data accessed through the OpenTopography portal (http://opentopography.org/). We compile 68 new measurements of lateral offset for displaced geomorphic features (Table 1; Haddon et al., 2012a, 2012b), and where possible, provide a direct comparison between field measurements and lateral offsets from the lidar data by analyzing specific geomorphic features described by previous workers (e.g., Carver, 1970; Beanland and Clark, 1994; Lee et al., 2001; Slemmons et al., 2008; Figure 1 and 2). The following analysis focuses on dextral offsets of geomorphic surfaces along the Owens Valley fault. The primary component of displacement in the 1872 earthquake was right-lateral, and occurred with an average ratio of ~6:1 relative to subordinate vertical offsets (Beanland and Clark, 1994).

Results

Table 1 summarizes our preliminary database of laterally offset geomorphic features for the Owens Valley fault. This table catalogs the location, magnitude, quality, and type of landform used to reconstruct fault slip. This database is also available as an ArcGIS shapefile and a Google Earth .kmz file in the Supporting Online Materials. We are also compiling detailed linework along the fault trace as a digital complement to mapping at 1:12,000 by Slemmons et al. (2008) based on low-sun-angle aerial photography. The published version of this report will include additional measurements currently pending field verification, in addition to measured vertical displacements catalogued for each feature.

To assess the spatial distribution of slip along the Owens Valley fault, we compile lateral offset measurements as a function of distance along the average fault strike of 340° (Figure 2a). If we

Table 1. Compiled lateral offset sites along the Owens Valley fault measured with GeoEarthscope lidar topography. References for field measurements are abbreviated as follows: BC – Beanland and Clark, 1994; KCM – Kirby et al., 2008; LPB – Lee et al., 2001.

Site	Latitude (deg)	Longitude (deg)	Sect.	Feature	Distance along fault (km)	Lidar Dextral Offset (m)	error (-, m)	error (+, m)	Quality	Field Dextral Offset (m)	± (m)
OL01	36.32058	-117.96348	S	shoreline	3.39					1.8	0.4
OL02	36.31984	-117.96296	S	shoreline	3.39					2.3	0.4
HA01612b	36.43771	-118.03703	S	channel	16.12	5.0	0.6	0.6	4		
HA01708a	36.43861	-118.03694	S	channel	17.08	8.0	0.7	0.7	5		
HA01714a	36.43921	-118.03684	S	channel	17.14	14.0	2.1	2.1	2		
HA01997a	36.46362	-118.03948	S	channel	19.97	1.7	0.4	0.4	4		
HA01997b	36.46358	-118.03970	S	channel	19.97	6.1	0.8	0.8	4		
HA02321a	36.49259	-118.04332	S	channel	23.21	7.1	0.6	0.6	5		
HA02374a	36.49700	-118.04440	S	channel	23.74	8.0	3.0	1.2	3		
HA03154a	36.56431	-118.06130	S	channel	31.54	12.6	1.6	2.4	2		
HA03158a	36.56468	-118.06148	S	channel	31.58	8.4	1.5	1.6	3		
BC05	36.56632	-118.06199	S	riser	32.22					13.1	2
HA03222a	36.56631	-118.06191	S	channel	32.22	4.7	1.0	1.0	4		
HA03222b	36.56627	-118.06190	S	channel	32.22	25	4	4	5		
HA03270a	36.57470	-118.06467	S	channel	32.7	20.8	3.4	2.7	2		
HA03290a	36.57238	-118.05729	S	fan axis	32.90	82	20	20	3		
HA03306a	36.58341	-118.07020	S	channel	33.06	6.0	1.1	1.1	3		
HA03395a	36.58346	-118.07245	S	channel	33.95	6.0	1.0	1.4	2		
HA03422a	36.58426	-118.07071	S	channel	34.22	2.1	0.7	0.7	4		
HA03482a	36.58425	-118.07289	S	channel	34.82	2.1	0.9	0.9	2		
BC07	36.60431	-118.06519	S	road	36.2					4.9	2
HA03745b	36.60711	-118.07652	S	fan axis	37.45	11	9	20	3		
HA03750a	36.60761	-118.07672	S	riser	37.5	12.0	1.0	1.0	3		
BC09S/HA03750b	36.60751	-118.07666	S	channel	37.50	7.5	1.5	1.5	3	6	2
BC09S/HA03750c	36.60748	-118.07664	S	riser	37.50	12.4	1.9	1.9	2	12	2
BC08	36.61560	-118.06704	S	treeline	37.6					2.7	2
HA03771a	36.60904	-118.07711	S	channel	37.71	16.7	2.0	2.0	3		
HA03771b	36.60886	-118.07703	S	channel	37.71	17.6	2.3	1.6	3		
BC09N	36.60978	-118.07743	S	channel	37.8					6	2
BC09N	36.60978	-118.07743	S	channel	37.80					8	2
BC09N	36.60978	-118.07743	S	channel	37.8					12	2
HA03827a	36.62810	-118.07476	C	channel	38.27	4.0	2.3	2.0	3		
LPB/HA03850a	36.63015	-118.07606	S	channel	38.50	6.7	1.1	1.6	2	8.9	0.8
LPB/HA03850b	36.63015	-118.07606	S	channel	38.50	13.1	0.3	0.3	2	12.9	0.2
HA04060a	36.64712	-118.09271	S	channel	40.60	6.0	0.8	0.8	3		
HA04069a	36.64778	-118.09299	S	channel	40.69	5.6	1.2	1.2	2		
HA04421a	36.67137	-118.09417	S	channel	44.21	6.5	0.6	0.6	5		
HA04457a	36.68584	-118.08967	C	channel	44.57	5.0	1.0	2.0	3		
HA04457b	36.68610	-118.08975	C	channel	44.57	4.5	1.4	1.4	2		
HA04991a	36.72385	-118.12528	C	channel	49.91	5.5	1.5	0.7	2		
HA05056a	36.72382	-118.12346	C	channel	50.56	3.8	0.8	0.8	4		
HA05071a	36.72470	-118.12571	C	channel	50.71	11.0	1.4	1.4	4		
HA05150a	36.74175	-118.11049	C	channel	51.50	5.5	1.1	1.1	4		
HA05212a	36.74678	-118.11265	C	channel	52.12	4.9	1.0	1.0	4		
HA05420b	36.75813	-118.11901	C	riser	54.20	4.4	2.2	2.4	2		
HA05421a	36.75830	-118.11908	C	riser	54.21	4.9	3.0	7.0	2		
HA05428a	36.75952	-118.11968	C	riser	54.28	2.4	1.1	1.1	3		
HA05430b	36.75942	-118.11956	C	riser	54.30	5.0	1.0	1.8	3	3	2
HA05450a	36.75990	-118.11983	C	riser	54.50	5.5	0.5	0.5	3	4	2
HA05500a	36.76609	-118.12245	C	riser	55.00	2.5	1.0	1.0	5		
HA05500c	36.76586	-118.1227	C	riser	55.00	22.4	2.9	2.1	4		
HA06320c	36.83535	-118.15511	C	channel	63.20	7.5	2.4	0.6	4	7	2
HA06433a	36.84721	-118.16223	C	channel	64.33	8.9	1.0	1.0	5		
HA06586a	36.85703	-118.16697	C	channel	65.86	8.0	0.7	1.3	3		
HA06599a	36.85871	-118.16785	C	channel	65.99	4.8	2.2	2.2	2		
HA07693c	36.95221	-118.20809	S	riser	76.93	65	15	5	3		
HA07693b	36.95193	-118.20798	C	riser	76.93	19	4	4	5		
HA07847a	36.96592	-118.21331	C	basin margin	78.47	71	12	12	5		
HA07964a	36.97588	-118.21701	C	riser	79.64	35	7	7	5		
HA08414a	37.01605	-118.22394	C	channel	84.14	4.0	1.3	1.3	5		
BC35	37.10414	-118.27280	N	terrace	95.2					10	2
HA09564a	37.11218	-118.27589	N	channel	95.64	10.5	2.3	1.5	3		
BC35	37.10414	-118.27280	N	ridge	95.7					30	2
HA09572a	37.11274	-118.27609	N	channel	95.72	7.9	1.9	1.9	4		
HA09938a	37.14260	-118.29212	N	channel	99.38	3.9	1.8	1.0	4		
HA09975a	37.14723	-118.29424	N	channel	99.75	4.2	0.8	0.8	2		
HA09994a	37.14961	-118.29582	N	channel	99.94	2.4	0.7	0.7	2		
HA09995a	37.14759	-118.29447	N	channel	99.95	2.3	0.7	0.7	3		
HA09997a	37.14983	-118.29589	N	channel	99.97	2.7	0.7	0.7	3		
HA10000a	37.15016	-118.29600	N	channel	100.00	6.2	0.7	0.8	3		
HA10005b	37.15096	-118.29488	N	channel	100.05	11.9	1.4	2.1	4		
HA10005a	37.15118	-118.29492	N	channel	100.05	7.9	0.9	1.8	3		
KCM	37.14609	-118.29442	N	flow margin	100.10					235	15
HA10029a	37.15287	-118.29611	N	channel	100.29	7.5	1.6	0.6	5		
HA10030a	37.15325	-118.29631	N	channel	100.34	17.2	1.8	1.8	5		
HA10034b	37.15355	-118.29649	N	riser	100.34	17.4	1.6	1.6	3		
HA10034c	37.15366	-118.29656	N	riser	100.34	17.3	1.8	1.8	3		
HA10236a	37.17062	-118.30233	N	channel	102.36	5.6	1.5	1.8	2		
HA10453a	37.18917	-118.30737	N	riser	104.53	10.8	1.4	1.4	3		

assume that peaks in the cumulative offset distribution correspond to frequent values of displacement related to past large earthquakes, surface slip during the most recent event (MRE) ranges between ~2 and ~8 m, with an average horizontal offset of 5.3 ± 2 m (Figure 2b). Measurements contributing to a subsidiary peak at ~2.5 m are observed near rupture endpoints and within zones of distributed faulting up to 3 km wide. As such, we consider these values to be minimum bounds on lateral slip during the MRE. If we exclude these smaller offsets, we calculate an average maximum displacement of 6.0 ± 1.5 m, in good agreement with field estimates from Beanland and Clark (1994). A subsidiary peak at ~8 m may likewise reflect slip variability at the northern end of the fault (Figure 2) smaller unrecognized events, or potentially triggered slip from nearby subparallel faults (Figure 1).

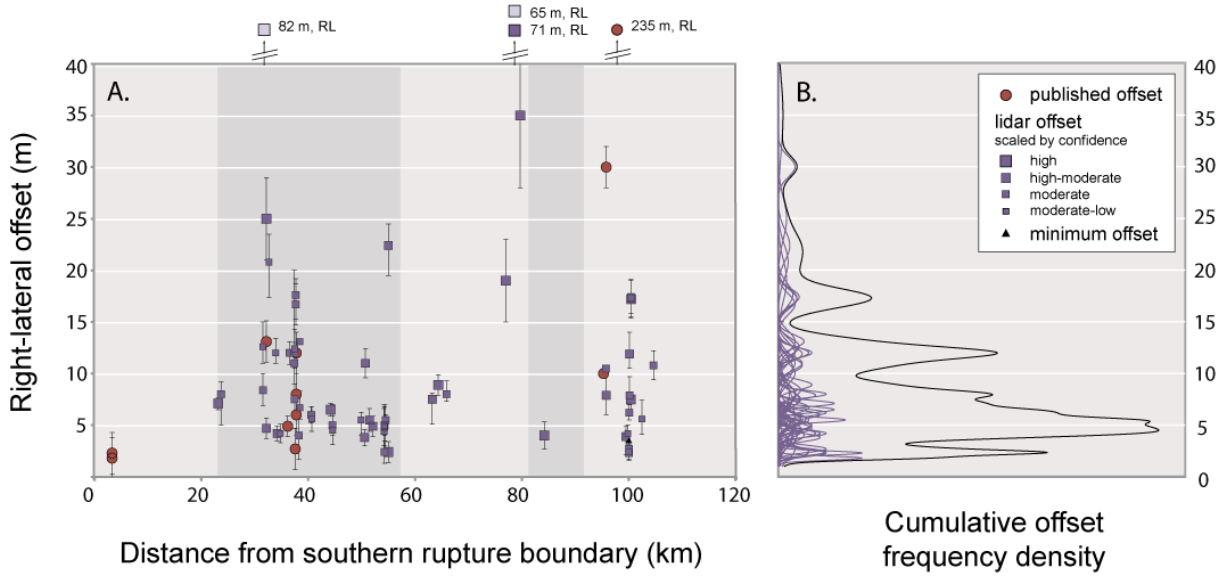

Figure 2. (A) Compilation of new and published measurements of dextrally offset landforms along the Owens Valley fault. Plot excludes measurements currently pending field assessment. Symbols for features identified using GeoEarthscope lidar (purple boxes) are scaled by quality ranking, from high to low. Published data (red points) are from Bateman (1961), Lubetkin and Clark (1987), Beanland and Clark (1994), Lee et al., (2001), Slemmons et al., (2008), and Kirby et al. (2008). Grey inset boxes highlight right-lateral offsets measured at sites within broad (1-3 km) zones of deformation. Measurements within these zones do not span the apparent width of deformation and may be regarded as minimum values. (B) Plot of cumulative offset frequency density for lateral offset measurements compiled on Figure 3a. The summary curve is peaked at values that may correspond to the most recent event (~6 m) and earlier surface ruptures (~12 and ~17 m). Small offsets (<3.5 m) are measured within zones of distributed deformation and contribute to a preliminary peak at ~2.5.

Provided that progressively larger offset groups reflect the recurrence of large surface ruptures (as opposed to the cumulative effects of smaller magnitude events), additional peaks in the cumulative offset frequency distribution (COFD) can be related to cumulative slip during the earlier earthquakes. Similar magnitudes of vertical offset during the penultimate and antepenultimate events observed in paleoseismic trenches on Owens Valley fault indicate the dominance of larger events similar to 1872, rather than smaller isolated ruptures (Bacon and Pezzopane, 2007). A prominent peak in the COFD occurs at ~12 m, possibly corresponding to the penultimate earthquake (PE), which occurred at ca. 10 ka (Bacon and Pezzopane, 2007). If so,

the total slip distribution implies a similar rupture length for 1872 and the PE (Figure 2a). A less-distinct peak of cumulative offsets that cluster at ~17 m may represent the antepenultimate event (APE, Figure 2b). These peaks may imply a similar magnitude of surface slip (~5 m) to the 1872 surface rupture, although we are working to refine our estimate of slip in earlier events.

The revised average value of lateral offset of ~5-6 m favors an estimated M_w 7.6 for the 1872 Owens Valley using the scaling relationships of Wells and Coppersmith (1994) and a fault width of ~20 km (Hough and Hutton, 2008). As such, anomalously high ground motions observed at regional distances may result from attenuation differences (Bakun, 2006; Hough and Hutton, 2008) or differences in the energetics of Owens Valley surface ruptures in comparison with San Andreas events.

Future Directions

This forms the basis of a MSc project (Haddon) currently underway at Western Washington University and was presented at the 2012 SCEC and AGU annual meetings (Haddon et al., 2012a, 2012b). Current work will merge additional field-checked offsets with this preliminary database, and also a compilation of vertical offset measurements at each site. We are also currently testing methods for building COFD plots taking into account distributed slip on subparallel strands of the Owens Valley fault zone. Our results will complement a growing body of information on the active tectonics and earthquake history of the Owens Valley fault and related structures (Amos et al., 2013). We will further characterize these newly identified geomorphic features by dating the landforms to develop a comprehensive inventory of fault slip-rates over the Late Pleistocene. These new data will span a critical gap in our knowledge of Owens Valley fault slip and enable us to directly test hypotheses related to the temporal constancy of strain release along the Owens Valley fault zone.

Supplementary Online Material

HA_OVF_PrelimOffsets_20130312.zip
HTML files and table of preliminary lateral offsets

HA_OVF_PrelimOffsets_20130312_SHP.zip
ArcGIS shapefile of preliminary lateral offsets

HA_OVF_PrelimOffsets_KMZ_20130312.zip
Google Earth .kmz file of preliminary lateral offsets

References

Amos, C. B., Lutz, A. T., Jayko, A. S., Mahan, S. A., Fisher, G. B., and Unruh, J. R., 2013, Refining the southern extent of the 1872 Owens Valley Earthquake rupture through paleoseismic investigations in the Haiwee area, southeastern California: Bulletin of the Seismological Society of America, v.103., no 2A.

Bacon, S. N., and Pezzopane, S. K., 2007, A 25,000-year record of earthquakes on the Owens Valley fault near Lone Pine, California: Implications for recurrence intervals, slip rates, and segmentation models: Geological Society of America Bulletin, v. 119, no. 7-8, p. 823-847.

Bakun, W.H., 2006, MMI Attenuation and Historical Earthquakes in the Basin and Range Province of Western North America: Seismological Society of America Bulletin, v. 96, p. 2206-2220.

Bateman, P.C., 1961, Willard D. Johnson and the Strike-Slip Component of Fault Movement in the Owens Valley, California: Seismological Society of America Bulletin, v. 51, p. 483-493.

Beanland, S., and Clark, M. M., 1994, The Owens Valley fault zone, eastern California, and surface rupture associated with the 1972 earthquake, U.S. Geologic Survey Bulletin 1982, 29 p.

Bierman, P. R., Gillespie, A. R., and Caffee, M. W., 1995, Cosmogenic ages for earthquake recurrence intervals and debris flow fan deposition, Owens-Valley, California: Science, v. 270, no. 5235, p. 447-450.

Carver, G. A., 1969, Quaternary Tectonism and Surface Faulting in the Owens Lake Basin, California, MSc. thesis: University of Nevada, Reno, 113 p.

dePolo, C. M., Clark, D. G., Slemmons, D. B., and Ramelli, A. R., 1991, Historical surface faulting in the Basin and Range Province, Western North-America - Implications for fault segmentation: Journal of Structural Geology, v. 13, no. 2, p. 123-136.

Haddon, E.K., C.B. Amos, and Burgmann, R., 2012a, Surface slip during large Owens Valley Earthquakes, Eos Trans. AGU, Fall Meet. Suppl., Abstract T31B-2342.

Haddon, E.K., C.B. Amos, and Burgmann, R., 2012b, Surface slip during large Owens Valley Earthquakes, Southern California Earthquake Center Annual Meeting, Palm Springs, CA, Poster 105.

Hough, S. E., and Hutton, K., 2008, Revisiting the 1872 Owens Valley, California, earthquake: Bulletin of the Seismological Society of America, v. 98, no. 2, p. 931-949.

Kirby, E., Anandakrishnan, S., Phillips, F., and Marrero, S., 2008, Late Pleistocene slip rate along the Owens Valley fault, eastern California: Geophysical Research Letters, v. 35, no. 1, p. 6.

Klinger, Y., Etchebes, M., Tapponnier, P., and Narteau, C., 2011, Characteristic slip for five great earthquakes along the Fuyun fault in China: Nature Geoscience, v. 4, no. 6, p. 389-392.

Lee, J., Rubin, C. M., and Calvert, A., 2001, Quaternary faulting history along the Deep Springs fault, California: Geological Society of America Bulletin, v. 113, no. 7, p. 855-869.

Lubetkin, L. K. C., and Clark, M. M., 1988, Late Quaternary activity along the Lone Pine fault, eastern California: Geological Society of America Bulletin, v. 100, no. 5, p. 755-766.

Working Group on California Earthquake Probabilities, 2008, The Uniform California Earthquake Rupture Forecast, Version 2 (UCERF 2), U.S. Geological Survey Open-File Report.

Sieh, K., 1996, The repetition of large-earthquake ruptures: Proceedings of the National Academy of Sciences of the United States of America, v. 93, no. 9, p. 3764-3771.

Slemmons, D. B., Vittori, E., Jayko, A. S., Carver, G. A., and Bacon, S. N., 2008, Quaternary fault and lineament map of Owens Valley, Inyo County, eastern California, Geological Society of America, Map and Chart 96, 25 p.

Zehfuss, P. H., Bierman, P. R., Gillespie, A. R., Burke, R. M., and Caffee, M. W., 2001, Slip rates on the Fish Springs fault, Owens Valley, California, deduced from cosmogenic Be-10 and Al-26 and soil development on fan surfaces: Geological Society of America Bulletin, v. 113, no. 2, p. 241-255.

Zielke, O., Arrowsmith, J. R., Ludwig, L. G., and Akciz, S. O., 2010, Slip in the 1857 and Earlier Large Earthquakes Along the Carrizo Plain, San Andreas Fault: Science, v. 327, no. 5969, p. 1119-1122.